Electronic Supplementary Information for

Thermal Stability of L-Cysteine-Protected Au_{25} Clusters: Interplay between Melting and Ligand Desorption

Michael A. Short[1], Alexey V. Verkhovtsev[2], Theodoros Pavloudis[1,3], Richard E. Palmer[1] and Andrey V. Solov'yov[2]

[1] Nanomaterials Lab, Mechanical Engineering, Swansea University, Bay Campus, Fabian Way, Swansea SA1 8EN, UK
[2] MBN Research Center, Altenhöferallee 3, 60438 Frankfurt am Main, Germany
[3] School of Physics, Faculty of Sciences, Aristotle University of Thessaloniki, GR-54124 Thessaloniki, Greece

Email to: verkhovtsev@mbnexplorer.com, R.E.Palmer@Swansea.ac.uk, solovyov@mbnresearch.com

1) Parameters of the CHARMM force field

The standard CHARMM force field[1] treats the covalent interactions within the harmonic approximation as:

$$U_{ij}^{(bond)} = k_{ij}^{b}(r_{ij} - r_0)^2 \#(1)$$

where k_{ij}^{b} is the force constant of the bond stretching and r_0 is the equilibrium covalent bond length. The potential associated with the change of a valence angle involving atoms i, j and k reads as:

$$U_{ijk}^{(angle)} = k_{ijk}^{a}(\theta_{ijk} - \theta_0)^2 \#(2)$$

where k_{ijk}^{a} is the force constant and θ_0 is the equilibrium angle. These parameters for the cysteine molecule and its bonding to the gold cluster are summarized in Tables S1 and S2. The corresponding optimised geometry of a deprotonated cysteine (with the hydrogen atom removed from the thiol group) is shown in Fig. S1.

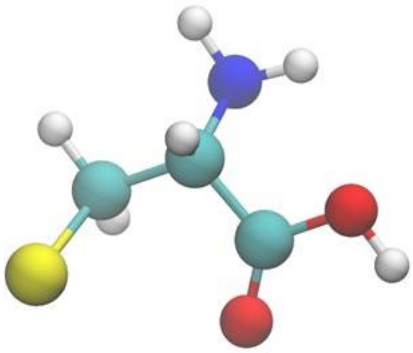

Figure S1. *Optimised structure of a deprotonated cysteine, which is considered as a ligand in the $Au_{25}Cys_{18}$ cluster.*

Table S1. *Parameters of the bonded interactions for a cysteine molecule used in the simulations.*

Bond	k_{ij}^{b} (kcal/mol Å^{-2})	r_0 (Å)
O–H	532.8	0.98
C–O(H)	417.5	1.36
C=O	932.0	1.22
C – C(O)	301.5	1.49
C–N	365.9	1.45
N–H	467.1	1.02
C–C	306.4	1.51
C–H	343.0	1.09
S–C	212.7	1.80
Au–S	200.0	2.42

The Au-S bonds have been considered reactive and were described using the reactive rCHARMM force field[2]. The radial part of bonded interactions is described in rCHARMM by means of the Morse potential:

$$U_{ij}^{(bond)} = D_{ij}\left[e^{-2\beta_{ij}(r_{ij}-r_0)} - 2e^{-\beta_{ij}(r_{ij}-r_0)}\right] \#(3)$$

where D_{ij} is the dissociation energy of the bond between atoms *i* and *j*, and $\beta_{ij} = \sqrt{k_{ij}^b / D_{ij}}$ determines the steepness of the potential. The dissociation energy D_{ij} for Au-S bond was set equal to 50 kcal/mol (~2.17 eV), according to Refs. [3,4]. The cutoff distance for bond breaking was set equal to 3 Å, beyond which the Au-S bond is broken and the molecular topology of the system changes. The rupture of covalent bonds during simulation automatically employs a modification of the potential functions for valence angles, see Ref. [2] for details.

Table S2. *Parameters of the angular interactions for a cysteine molecule and Au-S 'staples' in the $Au_{25}Cys_{18}$ cluster used in the simulations.*

Angle	k_{ijk}^a (kcal/mol rad^{-2})	θ_0 (deg)
C–O–H	42.0	111.9
O=C–O(H)	83.1	124.4
(H)O–C–C	75.1	109.7
O=C–C	67.5	124.4
N–C–C(O)	86.1	105.8
C–N–H	54.9	109.1
H–N–H	42.8	106.0
N–C–H	47.0	110.3
N–C–C	55.9	108.3
C–C–C(O)	55.9	107.5
(O)C–C–H	46.8	108.4
C–C–H	45.8	110.5
H–C–H	37.1	108.8
S–C–C	72.0	109.5
S–C–H	39.4	116.6
Au–S–C	500.0	109.0
S–Au–S	109.0	172.0
Au(inner)–S–Au(outer)	500.0	91.3
Au(outer)–S–Au(outer)	500.0	100.0

The angular interaction parameters for Au-S-C angles as well as for the angles within each Au-S staple (i.e. S-Au-S and Au-S-Au angles) were taken from Ref. [3], where these parameters were developed and used to simulate the structure and dynamics of various ligand-protected gold clusters.

The non-bonded van der Waals interaction between atoms of the ligands and gold atoms of the core is described using the Lennard–Jones potential:

$$U_{LJ} = \varepsilon_{ij}\left[\left(\frac{r_{min}}{r_{ij}}\right)^{12} - 2\left(\frac{r_{min}}{r_{ij}}\right)^{6}\right] \#(4)$$

where $\varepsilon_{ij} = \sqrt{\varepsilon_i \varepsilon_j}$ and $r_{min} = r_{min}(i)/2 + r_{min}(j)/2$. The corresponding parameters are listed in Table S3.

Table S3. *Parameters of the Lennard–Jones potential describing the van der Waals interaction between atoms of cysteine molecules with gold atoms in the $Au_{25}Cys_{18}$ cluster used in the simulations.*

Atom type	ε_i (kcal/mol)	$r_{min}/2$ (Å)
S	0.45	2.00
O(H)	0.1521	1.77
O(=C)	0.12	1.70
N	0.20	1.85
C	0.055	2.175
C(=O)	0.11	2.00
H(-C)	0.022	1.32
H(-N)	0.046	0.2245
H(-O)	0.046	0.2245
Au	5.2899	1.475

2) Structural Dynamics Analysis

To verify the stability of the presented results vs. simulation time, we have simulated the heating of the bare Au_{25} cluster at lower heating rates. In each simulation series, the temperature of the cluster was increased in steps of 20 K, and constant-temperature simulations were performed for each temperature for either 10 or 20 ns. The total simulation time in these additional simulations was therefore either 500 ns or 1000 ns (corresponding to the heating rates of 2 K/ns and 1 K/ns, respectively).

Figure S2 compares the results for the 4 ns-long NVT simulations (see Fig. 2(a) in the main text) with the new results obtained from 10 and 20 ns-long NVT simulations. The figure demonstrates that the rapid change in RMSD of the gold atoms is practically independent of simulation time within the considered range of values.

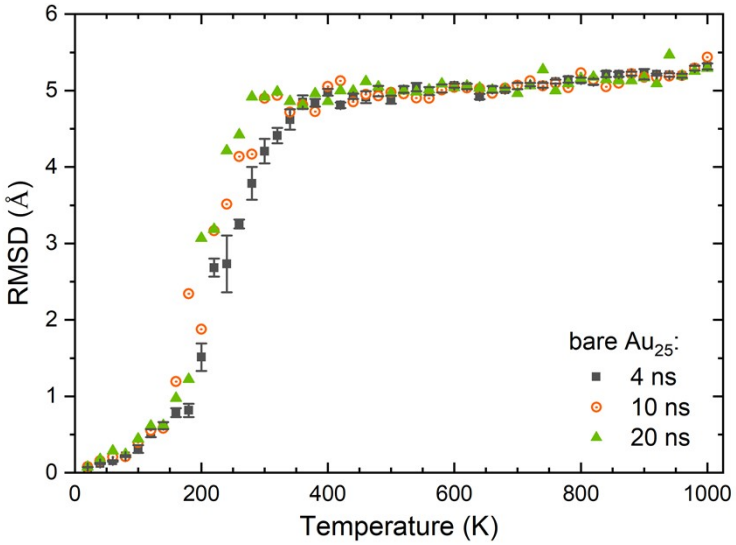

Figure S2. *RMSD profiles of the bare Au_{25} cluster calculated from 4 ns, 10 ns, and 20 ns-long NVT simulations.*

3) Energetic and Thermal Evolution of the $Au_{25}Cys_{18}$ Cluster

To further characterize the system's behaviour during heating, we analysed the evolution of key energy components and temperature over the course of the simulations. Figure S3 presents the time-dependent profiles of ***(a)*** the many-body energy due to interactions among gold atoms, ***(b)*** the bonded energy associated with covalently bonded atoms within the cysteine ligands and Au–S bonds, and ***(c)*** the instantaneous temperature of the system.

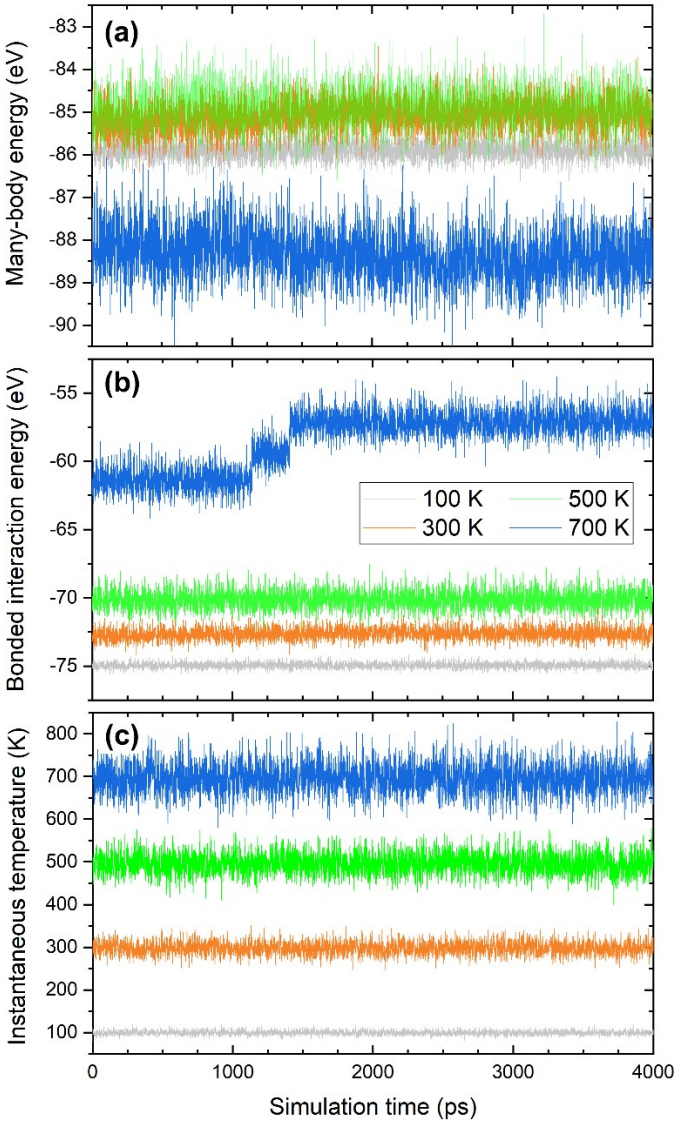

Figure S3. *Potential energy contributions (a,b) and instantaneous temperature (c) of the $Au_{25}Cys_{18}$ cluster versus simulation time. Panel (a) illustrates the behaviour of the many-body energy due to the interaction between all gold atoms. Panel (b) describes the evolution of the bonded energy, i.e. the energy involving all covalently bonded atoms within the cysteine ligands and in the Au-S bonds.*

At lower temperatures (T = 100, 300, and 500 K), both the many-body and bonded energy components gradually decrease (in absolute magnitude) and fluctuate around stable average values, indicating a well-equilibrated system. At T = 700 K, a notable drop in the many-body energy is observed, suggesting a structural phase transition within the gold core. Concurrently, the bonded energy profile exhibits stepwise changes, corresponding to the progressive breaking of Au–S bonds and the detachment of cysteine ligands. This analysis complements the structural metrics presented in the main text and provides further insight into the thermal and energetic stability of the $Au_{25}Cys_{18}$ cluster across different temperature regimes.

During the simulations, both atomic coordinates and velocities were recorded at different simulation steps. These data were analysed using the built-in tools of MBN Studio software package [5] to compute the kinetic energy distribution of the system. Figure S4 presents the kinetic energy distribution of the gold atoms within the $Au_{25}Cys_{18}$ cluster at four representative temperatures: 100 K, 300 K, 500 K, and 700 K.

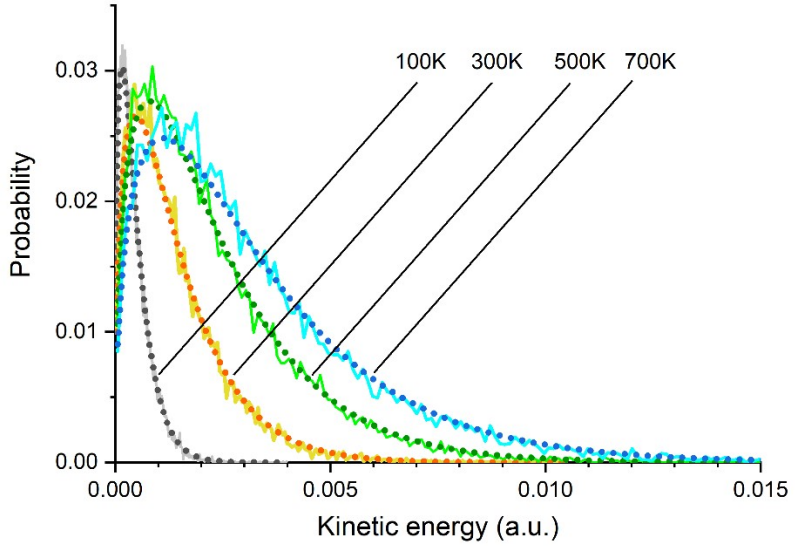

Figure S4. *The kinetic energy distribution for the gold atoms of the $Au_{25}Cys_{18}$ cluster at different temperatures as indicated. Solid lines show the distributions calculated directly from the simulated trajectories. Dotted lines show the Maxwell-Boltzmann distribution calculated analytically using Eq. (5).*

All simulations in this study were carried out in the NVT statistical ensemble. The system temperature was regulated using a Langevin thermostat, ensuring that particle velocities follow the Maxwell–Boltzmann distribution. The corresponding probability distribution of the kinetic energy is expressed as:

$$f(E) = 2\sqrt{\frac{E}{\pi}}\left(\frac{1}{k_B T}\right)^{3/2} exp\left(-\frac{E}{k_B T}\right) \#(5)$$

where E denotes the kinetic energy of the molecular system, T the temperature, and k_B the Boltzmann constant. The kinetic energy distributions obtained directly from 4 ns simulation trajectories (solid lines in Fig. S4) are in close agreement with the theoretical Maxwell–Boltzmann distributions defined by Eq. (5) (dotted lines), confirming the correct thermalization of the system under the chosen simulation conditions.

4) Discussion on the Melting Points of sub-1 nm clusters

One cannot easily compare the melting temperature cited for the Au_{25} clusters in this work with previous experimental data of larger nanoparticles since no safe extrapolation for the melting of very small nanoparticles like the Au_{25}.

Font and Myers investigated the melting of spherically symmetric nanoparticles and found that both the standard and their own expression of the Gibbs–Thomson equation, despite providing very good fits for the experimental data of Buffat and Borel [6], fail for nanoparticles under 1 nm [7]. The authors concluded that "the generalised Gibbs–Thomson relation should not be applied below this value" and cut-off their solutions at $r = 1\,nm$.

For example, a simple Gibbs-Thompson relation fitted on the experimental data of Buffat and Borel would take the form of:

$$T_m = 1337\left(1 - \frac{0.49}{r}\right)$$

and would return a negative, unphysical value for our ~0.4 nm-radius Au_{25} NPs.

Additionally, the Gupta potential [8] used in the present study, despite overestimating the melting temperature of Ni, Ag, Cu, Co by 10%, "considerably underestimates" the phonon cutoff frequencies and the melting temperature of Au [9].

It is worth noting that the melting temperature of Au_{25} predicted in this study is close to the melting temperatures of slightly larger gold clusters (Au_{30}–Au_{50}), as determined by MD simulations using the Gupta potential [10]. Reported values of melting temperature vary from (260 ± 50) K for Au_{35} to (330 ± 20) K for Au_{50}.

References

[1] A. D. Mackerell *et al.*, "All-atom empirical potential for molecular modeling and dynamics studies of proteins", *J. Phys. Chem. B*, 1998, **102**, 3586–3616.

[2] G. B. Sushko, I. A. Solov'yov, A. V. Verkhovtsev, S. N. Volkov, and A. V. Solov'yov, "Studying chemical reactions in biological systems with MBN Explorer: Implementation of molecular mechanics with dynamical topology", *Eur. Phys. J. D*, 2016, **70**, 12.

[3] E. Pohjolainen, X. Chen, S. Malola, G. Groenhof, and H. Häkkinen, "A unified AMBER-compatible molecular mechanics force field for thiolate-protected gold nanoclusters", *J. Chem. Theory Comput.*, 2016, **12**, 1342–1350.

[4] A. V. Verkhovtsev, A. Nichols, N. J. Mason, and A. V. Solov'yov, "Molecular dynamics characterization of radiosensitizing coated gold nanoparticles in aqueous environment", *J. Phys. Chem. A*, 2022, **126**, 2170–2184.

[5] G. B. Sushko, I. A. Solov'yov, and A. V. Solov'yov, "Modeling MesoBioNano systems with MBN Studio made easy", *J. Mol. Graph. Model.*, 2019, **88**, 247–260.

[6] Ph. Buffat and J-P. Borel, "Size effect on the melting temperature of gold particles", *Phys. Rev. A*, 1976, **13**, 2287–2298.

[7] F. Font and T. G. Myers, "Spherically symmetric nanoparticle melting with a variable phase change temperature", *J. Nanopart. Res.,* 2013, **15**, 2086.

[8] F. Cleri and V. Rosato, "Tight-binding potentials for transition metals and alloys", *Phys. Rev. B*, 1993, **48**, 22–33.

[9] G. B. Sushko, A. V. Verkhovtsev, Ch. Kexel, A. V. Korol, S. Schramm, and A. V. Solov'yov, "Reconciling simulated melting and ground-state properties of metals with a modified embedded-atom method potential", *J. Phys.: Condens. Matter*, 2016, **28**, 145201.

[10] D. Schebarchov, F. Baletto, and D. J. Wales, "Structure, thermodynamics, and rearrangement mechanisms in gold clusters – insights from the energy landscapes framework", *Nanoscale*, 2018, **10**, 2004-2016.